Ω characterizes the degree of flow unsteadiness by representing the largest amplitude of the cross-plane velocity sum along the centerline. Figure 2b shows that Ω departs from zero at the same value of $\mathcal{V}$ that the flow becomes asymmetric. Thus, Figs. 2a and 2b demonstrate that flow unsteadiness and asymmetry are intimately linked. The loss of stability to time-periodic flow is evidence for a Hopf bifurcation. The bifurcation is supercritical,[8] since the amplitude of the disturbance, characterized by Ω, grows from zero as $\mathcal{V}$ is increased past the Hopf point. The initial and final values of Q are shown in Fig. 2c. A region in $\mathcal{V}$ exists where two-dimensional flows with bubble-type breakdown evolve into three-dimensional, unsteady flows with no reversed flow. Also, it is of interest to note that the Hopf point and the appearance of reversed flow occur at different values of $\mathcal{V}$. Thus, loss of stability is not a consequence of a gross structural change in the flowfield. Other examples in which changes in flowfield topology are disassociated from hydrodynamic bifurcations are given by Lopez.[3]

The observed increase in Q as the flow transitions from two- to three-dimensional flow is correlated to a particular asymmetric term in the governing equations. Details of this analysis can be found in Ref. 5. The correlation requires concepts put forth by Brown and Lopez[9] and Darmofal.[10] Brown and Lopez[9] established a necessary condition between the production of negative azimuthal vorticity $\hat{\eta}$ and the extent of axial flow deceleration. Consequently, the authors anticipated that the minimum azimuthal vorticity for the three-dimensional flow would be greater (less negative) than that of the initial two-dimensional flow, since Q is greater in these cases. This is indeed the case. At $\mathcal{V} = 1.5$, before the Hopf bifurcation, the minimum values of $\hat{\eta}$ computed from both the two- and three-dimensional models are virtually the same. However, just beyond the Hopf point, the minimum $\hat{\eta}$ is significantly greater in the three-dimensional flow. A numerical evaluation of asymmetric terms in the azimuthal vorticity equation is then performed.[5] This equation relates the total derivative of $\hat{\eta}$ to vorticity stretching and tilting terms.[10] Through this evaluation, it is found that the effect of three-dimensionality on radial vorticity is the principle contributor to the increase in $\hat{\eta}$. A region consisting of a positive net change in radial vorticity exists that serves to attenuate the axial deceleration process.

Flowfield visualization is performed by calculating the numerical equivalent of streaklines. Five material points are introduced into the flowfield at the inflow boundary. The white point lies initially on the tube centerline, whereas the grey scaled points lie on the y and z axes at nondimensional distances of ± 0.1 from the centerline. The material point positions are computed in time from the evolving velocity field using a first-order-accurate Euler time integration.[4] Snapshots of the time-asymptotic streaklines are shown in Fig. 3; the tube geometry is omitted for clarity. Figure 3 shows the development of three-dimensional flow as $\mathcal{V}$ is increased past the Hopf bifurcation point. At $\mathcal{V} = 2.3$ (Fig. 3d), the material points deflect off-axis in a well-defined helical-type structure, consistent with spiral-type breakdown. Further discussion of the flow visualization can be found in Ref. 5.

Conclusions

Time integration of the three-dimensional, compressible Navier–Stokes equations reveals that when the vortex strength is increased past a critical value, the time-asymptotic flow changes from axisymmetric and steady to asymmetric and time periodic, indicating a supercritical Hopf bifurcation. The three-dimensional flows form a solution branch that bifurcates from the path of two-dimensional solutions at the bifurcation point. The authors' interpretation of this result is that the mechanism for the existence of a least one family of three-dimensional solutions, which possess reversed flow at sufficiently large values of vortex strength, is the loss of stability of the axisymmetric base flows. Minimum values of axial velocity Q are observed to increase as flow asymmetries develop just beyond the Hopf point. Furthermore, a small range of $\mathcal{V}$ exists where two-dimensional solutions exhibit vortex breakdown but three-dimensional solutions do not. This attenuation of axial deceleration is found by the authors to be the result of a positive net production of radial vorticity as flow asymmetries develop.

References

[1]Leibovich, S., and Kribus, A., "Large-Amplitude Wavetrains and Solitary Waves in Vortices," *Journal of Fluid Mechanics*, Vol. 216, July 1990, pp. 459–504.

[2]Beran, P. S., and Culick, F. E. C., "The Role of Non-Uniqueness in the Development of Vortex Breakdown in Tubes," *Journal of Fluid Mechanics*, Vol. 242, Sept. 1992, pp. 491–527.

[3]Lopez, J. M., "On the Bifurcation Structure of Axisymmetric Vortex Breakdown in a Constricted Pipe," *Physics of Fluids*, Vol. 6, No. 11, 1994, pp. 3683–3693.

[4]Tromp, J. C., "The Dependence of the Time-Asymptotic Structure of 3-D Vortex Breakdown on Boundary and Initial Conditions," Ph.D. Dissertation, Dept. of Aeronautics and Astronautics, U.S. Air Force Inst. of Technology, Wright–Patterson AFB, OH, 1995.

[5]Tromp, J. C., and Beran, P. S., "Temporal Evolution of Three-Dimensional Vortex Breakdown from Steady, Axisymmetric Solutions," AIAA Paper 95-2310, June 1995.

[6]Lele, S. K., "Compact Finite Difference Schemes with Spectral-Like Resolution," *Journal of Computational Physics*, Vol. 103, Nov. 1992, pp. 16–42.

[7]Faler, J. H., and Leibovich, S., "Disrupted States of Vortex Flow and Vortex Breakdown," *Physics of Fluids*, Vol. 20, No. 9, 1977, pp. 1385–1400.

[8]Seydel, R., *From Equilibrium to Chaos: Practical Bifurcation and Stability Analysis*, Elsevier, New York, 1988.

[9]Brown, G., and Lopez, J., "Axisymmetric Vortex Breakdown, Part 2: Physical Mechanisms," *Journal of Fluid Mechanics*, Vol. 221, Dec. 1990, pp. 553–576.

[10]Darmofal, D. L., "The Role of Vorticity Dynamics in Vortex Breakdown," AIAA Paper 93-3036, July 1993.

Finite Element Analysis of Laminated Composites Using an Unmixing–Mixing Viscoplastic Model

Seung-Jo Kim* and Eui-Sup Shin†
Seoul National University,
Seoul 151-742, Republic of Korea

Introduction

ADVANCED composites in high-temperature environments, e.g., various aerospace applications, exhibit inelastic behavior such as creep and plasticity interaction. For example, thermoplastic composites have improved fracture and damage tolerance properties owing to the increased matrix ductility. Also, metal matrix composites show an appreciable viscoplastic deformation in severe thermal conditions. Therefore, characterizing the viscoplasticity is indispensable for reliable analysis and design of composite structures in such environments.

However, the intrinsic nonlinearity of viscoplastic phenomena and the anisotropy of composite materials increase difficulties in analyzing the viscoplastic behaviors. Many kinds of constitutive models were proposed to simulate the rate-dependent plasticity of composite materials. Most of them were modified or/and extended from classical or the unified viscoplastic models of isotropic materials.[1–3] However, these macroscopic theories fundamentally have some disadvantages in identifying the constitutive relations. Mainly, it is difficult and self-empirical to determine the appropriate form of anisotropic functions (or functionals) with vector and tensor invariants required in a yield criterion, flow potential, dissipation energy potential, etc. From a practical viewpoint, evaluating various material constants used in the macroscopic equations is very expensive and time-consuming.

Received Oct. 31, 1994; revision received Oct. 10, 1995; accepted for publication Oct. 30, 1995.

*Professor, Department of Aerospace Engineering. Member AIAA.
†Graduate Research Assistant. Member AIAA.

Up to now, there have been a few works in plasticity theory based on a micromechanics model that derives the overall composite behavior from the properties of the constituents.[4] Recently, Kim and Cho[5] proposed a new concept, unmixing and mixing, to investigate the role of a matrix in the viscoplastic behavior of thermoplastic composite. This concept made use of the viscoplastic rule of an isotropic matrix material and not the complex and expensive viscoplastic rule of an anisotropic material.

In this work, the unmixing–mixing scheme is illustrated briefly. Then, the boundary-value problem for composite laminates is formulated with the principle of virtual work. To solve the derived nonlinear equations including contact boundary, the finite element methods with a penalty parameter are applied. As a numerical example, the bolted joint problem of laminated composites is solved by a developed computer code.

Unmixing–Mixing Elastoviscoplastic Model

The unmixing–mixing scheme is applied to describe the elastoviscoplastic behavior of orthotropic composite materials. Here, only the equations needed in the finite element calculations are presented in appropriate forms.

First, the strain rate at a local material point can be written in tensor form,

$$\dot{\boldsymbol{\varepsilon}} = \dot{\boldsymbol{\varepsilon}}^e + \dot{\boldsymbol{\varepsilon}}^p = \boldsymbol{A}\dot{\boldsymbol{\sigma}} + \boldsymbol{B}\dot{\boldsymbol{\varepsilon}}_m^p \tag{1}$$

where superscripts e and p represent the elastic and viscoplastic components, respectively, and subscript m the matrix part. $\boldsymbol{A}$ is the typical elastic compliance tensor under the plane-stress condition, and the fourth-order tensor $\boldsymbol{B}$ relates the matrix plastic deformation to the overall plastic response of composite.

On the other hand, the stress rate undertaken by the matrix part have the following form:

$$\dot{\boldsymbol{\sigma}}_m = \boldsymbol{C}\dot{\boldsymbol{\sigma}} + \boldsymbol{D}\dot{\boldsymbol{\varepsilon}}_m^p \tag{2}$$

The first term is the rate of matrix microstress contributed from the overall loading and the second from the matrix plasticization. Since the unmixing–mixing equations (1) and (2) mean that $\dot{\boldsymbol{\varepsilon}} = fn(\dot{\boldsymbol{\sigma}}, \dot{\boldsymbol{\varepsilon}}_m^p)$ and $\dot{\boldsymbol{\sigma}}_m = fn(\dot{\boldsymbol{\sigma}}, \dot{\boldsymbol{\varepsilon}}_m^p)$, if we determine a matrix viscoplastic model $\dot{\boldsymbol{\varepsilon}}_m^p = fn(\boldsymbol{\sigma}_m)$, then we can relate stress to strain completely.

To bring the unmixing–mixing scheme to completion, any isotropic flow rule may be applied to the matrix viscoplastic model. In this work, a modified Bodner-Partom theory[6] is adopted. The resulting expressions for the flow rule are as follows:

$$\dot{\boldsymbol{\varepsilon}}_m^p = \frac{D_o}{2h_m\sqrt{J_m}} \exp\left(-\frac{Bh_m^{2n}}{J_m^n}\right)\boldsymbol{S}_m \tag{3}$$

$$h_m = h_1 + (h_0 - h_1)\exp(-m\Lambda_m) \tag{4}$$

$$\dot{\Lambda}_m = (1/h_m)\boldsymbol{S}_m : \dot{\boldsymbol{\varepsilon}}_m^p \tag{5}$$

where $\boldsymbol{S}$ is the deviatoric stress, J the second invariant of $\boldsymbol{S}$, Λ an internal state variable characterizing isotropic hardening effects, and h a hardness variable that is conjugate to Λ. D_o, h_0, h_1, m, n, and B are material constants for the isotropic matrix.

Finite Element Approximations

Variational formulation is set up to simulate the elastoviscoplastic behavior of composite laminates under the assumptions of infinitesimal, quasistatic, and isothermal conditions. This class of initial-boundary-value problems is governed by the following system of equations: G1) equilibrium state and plane stress condition in domain Ω, G2) displacement and kinematic relation in Ω, G3) constitutive relation with unmixing–mixing equations in Ω, G4) traction condition on boundary Γ_T, G5) displacement condition on boundary Γ_D, and G6) contact condition on boundary Γ_C.

Virtual displacements are applied to the equilibrium state in G1 and G4, which vanish on Γ_D to satisfy G5,

$$-\int_\Omega (\sigma_{ij,j} + \bar{f}_i)\delta u_i \, d\Omega + \int_{\Gamma_T} (\sigma_{ij}n_j - \bar{t}_i)\delta u_i \, d\Gamma_T + \frac{1}{\varepsilon}\int_{\Gamma_C} \langle u_j n_j - s\rangle n_i \delta u_i \, d\Gamma_C = 0 \tag{6}$$

where s is a initial contact clearance, ε a small positive number, and $\langle\,\rangle$ a bracket function. The third term in Eq. (6) can be recognized as the virtual expression due to the exterior penalty functional[7] for G6. The exterior penalty method is adopted in the current constrained formulation because it has a more relatively simple form of functional than other methods. The isoparametric finite element method is introduced with the displacement interpolation matrix $[H]$ and strain-displacement matrix $[B]$. Then, the discretized governing equations are written as follows:

$$([K] + [Q_1])\{U\} = \{F\} + \{P\} + \{Q_2\} \tag{7}$$

where $[K]$ is the global stiffness matrix, $\{F\}$ the global load vector, and

$$\{P\} = \int_\Omega [B^T][A^{-1}]\{\varepsilon^p\} \, d\Omega \tag{8}$$

$$[Q_1] = \frac{1}{\varepsilon}\int_{\Gamma_C} [H^T]\{n\}\{n^T\}[H] \, d\Gamma_C \tag{9}$$

$$\{Q_2\} = \frac{1}{\varepsilon}\int_{\Gamma_C} s[H^T]\{n\} \, d\Gamma_C \tag{10}$$

The integrations on Γ_C are performed only where $u_i n_i - s$ are positive.

The nonlinear equation (7) is put into an incremental form for a given time step Δt

$$[K]\{\Delta U\} + [Q_1]\{U\} = \{\Delta F\} + \{\Delta P\} + \{Q_2\} \tag{11}$$

Since the determination of $\{\Delta P\}$, $[Q_1]$, and $\{Q_2\}$ requires the knowledge of current state, the equilibrium is approximated and is achieved through successive iteration processes. The relative error of displacement increments is used as the convergence criterion.

The fast convergence of equilibrium iterations depends largely on how accurate the plastic strain increment $\Delta\varepsilon^p$ is calculated at all Gauss integration points. The unmixing–mixing equations are used to calculate the rate of overall plastic strain. Because of the inherent stiff phenomenon of viscoplastic rate equations, a subincrementing technique[8] is adopted at each integration point. The one-step forward Euler method appears to be suitable, provided that the global time step Δt is finely subdivided. This algorithm allows us to select the larger overall time intervals, without invoking any numerical instability due to stiff viscoplastic rate equations.

Numerical Results

To demonstrate the characteristics of the adopted viscoplastic theory and verify the effectiveness of the finite element schemes, the pin-loaded joint problem of a composite laminate is solved by the developed computer code. To simplify the problem, the assumptions of a rigidly fixed pin and perfect fastener to hole fit ($s = 0$) are made. In addition, we assume that the pin transfers to the laminate only through normal stresses over the contact area; that is, the shear stresses resulting from friction are neglected.

As shown in Fig. 1a, the specimen has the dimension of length 400 mm, width 160 mm, and hole radius 10 mm. The center of the circular hole is 60 mm from the upper-side edge. The laminated plate is composed of 8 laminas, i.e., $[15/-15/45/-45]_s$, and the thickness of each lamina is 1.25 mm. Thermoplastic composite AS4/PEEK is selected as the material system, and the ambient temperature is set to 121°C. The values of elastic moduli and viscoplastic constants

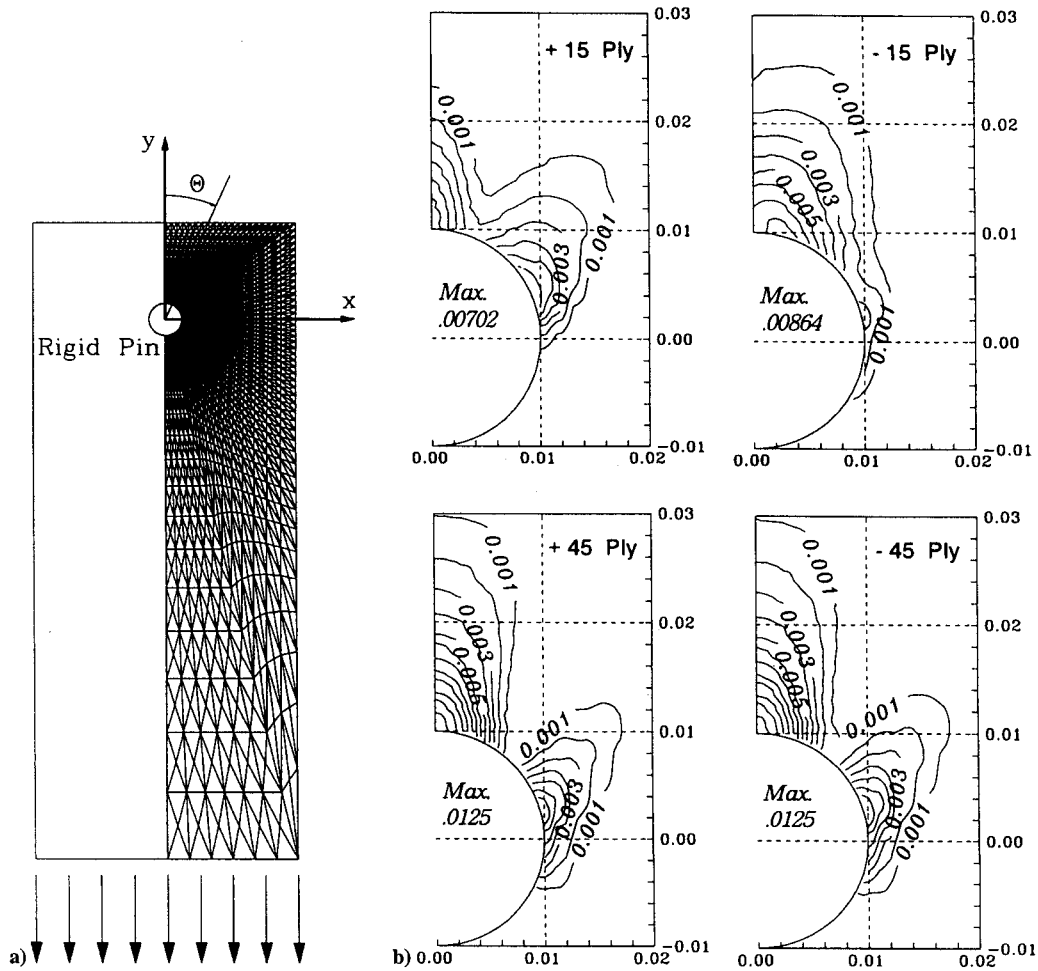

Fig. 1 Contours of viscoplastic deformation in plies: a) finite element mesh and b) $\sqrt{[\frac{1}{2}(\varepsilon_x^{p2} + \varepsilon_y^{p2}) + \frac{1}{4}\gamma_{xy}^{p2}]}$ at $t = 30$ s.

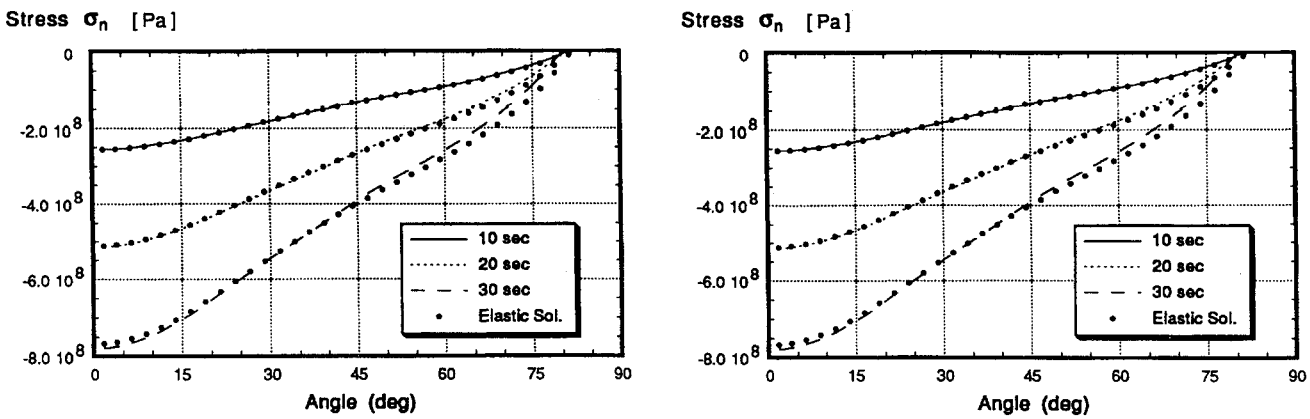

Fig. 2 Distributions of average stresses $\bar{\sigma}_n$ and $\bar{\sigma}_\theta$.

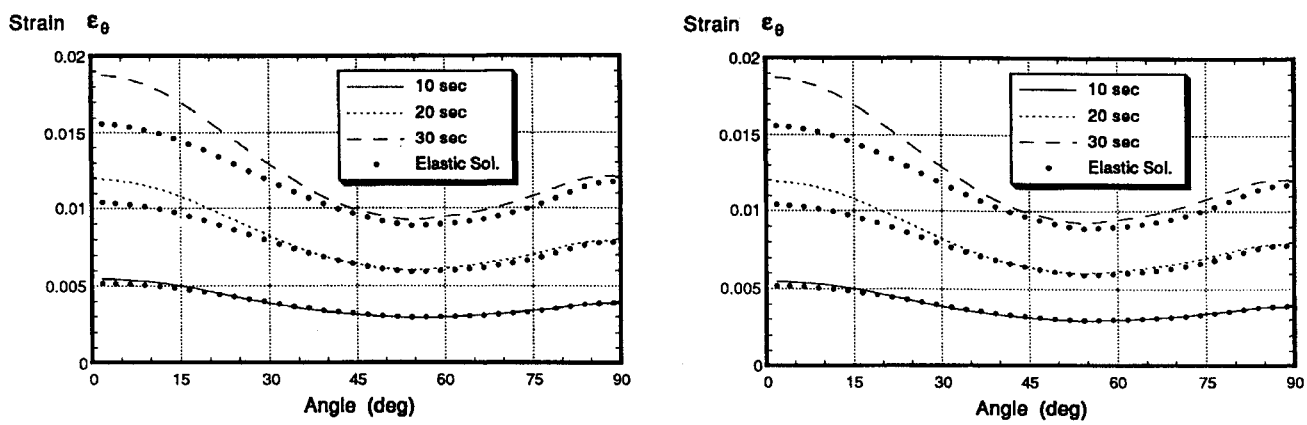

Fig. 3 Distributions of total strains $\bar{\varepsilon}_n$ and $\bar{\varepsilon}_\theta$.

are listed in Ref. 5. The right-half of the laminate is discretized by 1152 4CST (constant strain triangle) elements with 2393 node points as a finite element model. Sufficiently finer meshes are used in the vicinity of the hole. Uniform traction forces along the lower edge of the plate are linearly increased up to the maximum average stress $\bar{\sigma}_x = 75$ MPa for 30 s. The interval of the time steps is 0.25 s, and the number of subdivisions that are required for the numerical integration of viscoplastic rate equations is 200 within each global time step. Also, the error tolerance for convergence checking is fixed at 0.02%.

To view the propagation of inelastic deformation in laminates, maps of viscoplastic strain are drawn in Fig. 1b. One of the tensor invariants is selected as a measure of viscoplastic deformation. The plastic deformation spreads near the upper hole boundary in the initial stage because the contact force is largest at that region. At the subsequent time events, the portions that experience the inelastic deformation are gradually widened in all plies. The values of the plastic strain remain high on the hole boundaries in the $\theta = 0$ and 75 directions. Based on this information, it can be considered that the bearing mode will dominate the failure mechanisms of this composite structure with increased load conditions.

Distributions of the normal tractions in the radial and tangential directions are plotted in Fig. 2. The graph of the contact traction $\bar{\sigma}_n$ shows that the contact area varies slightly, about $\theta = 82$ deg when contact clearance is zero. Also the $\bar{\sigma}_\theta$ variations of the viscoplastic analysis deviate from the elastic solutions in $\theta = 0 \sim 15$ range. Figure 3 plots the variations of total strains. The differences between the elastic and elastoviscoplastic solutions are large at $\theta = 0$ and 75 deg, which illustrates that plastic flow in some part of the composite will produce more intense deformations of the structure.

Conclusions

An unmixing–mixing scheme is applied to describe the macroscopic viscoplastic behavior of composite materials. In computational aspects, the penalty finite element methods have provided convenient analysis capabilites for the elastoviscoplastic response of composite structures with complex geometry and boundary condition. The pin-jointed composite plate is solved as a numerical example to illustrate the basic characteristics of the proposed constitutive theory and the analysis capabilities of the numerical methods. The results have shown the propagations of inelastic deformation, the stress distributions in the plies, and the effects of viscoplastic phenomena that are different from the pure elastic cases. Research work, in which a failure criterion consistent with the unmixing–mixing scheme is included for finite element analysis, is in progress and will be reported on in a subsequent paper.

References

[1]Robinson, D. N., and Duffy, S. F., "Continuum Deformation Theory for High-Temperature Metallic Composites," *Journal of Engineering Mechanics*, Vol. 116, No. 4, 1990, pp. 832–844.

[2]Yoon, K. J., and Sun, C. T., "Characterization of Elastic-Viscoplastic Properties of an AS4/ PEEK Thermoplastic Compsite," *Journal of Composite Materials*, Vol. 25, 1991, pp. 1277–1296.

[3]Saleeb, A. F., and Wilt, T. E., "Analysis of the Anisotropic Viscoplastic-Damage Response of Composite Laminates—Continuum Basis and Computational Algorithms," *International Journal for Numerical Methods in Engineering*, Vol. 36, 1993, pp. 1629–1660.

[4]Dvorak, G. J., and Bahei-El-Din, Y. A., "Plasticity Analysis of Fibrous Composites," *Journal of Applied Mechnics*, Vol. 49, 1982, pp. 327–335.

[5]Kim, S. J., and Cho, J. Y., "Role of Matrix in Viscoplastic Behavior of Thermoplastic Composites at Elevated Temperature," *AIAA Journal*, Vol. 30, No. 10, 1992, pp. 2571–2573.

[6]Kim, S. J., and Oden, J. T., "Finite Element Analysis of a Class of Problems in Finite Elastoplasticity Based on the Thermodynamical Theory of Materials of Type N," *Computer Methods in Applied Mechanics and Engineering*, Vol. 53, 1985, pp. 277–302.

[7]Oden, J. T., and Kikuchi, N., "Finite Element Methods for Constrained Problems in Elasticity," *International Journal for Numerical Methods in Engineering*, Vol. 18, 1982, pp. 701–725.

[8]Chang, T. Y., Chen, J. Y., and Chu, S. C., "Viscoplastic Finite Element Analysis by Automatic Subincrementing Technique," *Journal of Engineering Mechanics*, Vol. 114, 1988, pp. 80–96.

Supersonic Flutter Analysis of Stiffened Isotropic and Anisotropic Panels

Dong-Min Lee* and In Lee†
Korea Advanced Institute of Science and Technology, Taejon 305-701, Republic of Korea

I. Introduction

PANEL flutter is a self-excited oscillating phenomenon and involves interactions among elastic, inertia, and aerodynamic forces. Many researchers have studied panel flutter problems for isotropic and anisotropic panels. Dowell[1] gave a comprehensive overview of panel flutter. Applications of the finite element method to linear flutter problems for isotropic panels have been presented by many investigators.[2,3] Recently, for high-performance and advanced aerospace structures, the use of laminated structural components has considerably increased. Hence, various studies[3–6] have been performed for supersonic flutter analysis of anisotropic panels by considering the effects of panel geometry, boundary conditions, lamination scheme, flow directions, and thermal effects.

Also for high-performance applications, the weight saving is an important consideration. It is often necessary to minimize the maximum deflection of skin panel without introducing any considerable weight penalty. This can be achieved by adding stiffeners to the skin panel. Many studies are available on vibration analysis of isotropic panels. However, studies on the vibration and flutter analysis of stiffened anisotropic panels are rare.

In the present study, flutter analysis of a stiffened panel has been performed using the structural model[7] proposed by the present authors to study the vibrational characteristics of anisotropic plates with stiffeners that are stacked vertically with respect to the skin panel. This paper investigates the effects of the stiffener size and the fiber orientation on the flutter boundaries.

II. Governing Equation for Flutter Analysis

A first-order shear-deformable plate model for skin panel and a Timoshenko beam model for stiffeners are used in the finite element modeling of the stiffened anisotropic panel. The plate and beam finite elements have nine and three nodal points, respectively. The plate and beam elements are connected through the appropriate kinematic relations between the skin panel and stiffener.[7]

The aerodynamic pressure exerted on deflected panel at a supersonic speed can be obtained using linearized piston theory. The aerodynamic stiffness and damping matrices in flutter calculations can be derived using the virtual work done by the aerodynamic forces. The resulting finite element equations can be obtained for the entire system as follows[4–6]:

$$[M]\{\ddot{U}\} + g[A_d]\{\dot{U}\} + ([K] + \beta[A_f])\{U\} = \{0\} \tag{1}$$

where $[M]$, $[K]$, and $\{U\}$ are the mass and stiffness matrices and the displacement vector, respectively; $[A_d]$ and $[A_f]$ are the aerodynamic damping and stiffness matrices, respectively; and β and g are the aerodynamic pressure and damping parameter, respectively. Assuming $\{U\} = e^{\omega t}\{U\}$, and transforming Eq. (1) to the state-space form, one can get the following equation:

$$\left(\begin{bmatrix} [0] & [M] \\ [K] + \beta[A_f] & g[A_d] \end{bmatrix} - \omega \begin{bmatrix} [M] & [0] \\ [0] & -[M] \end{bmatrix} \right) \begin{Bmatrix} U \\ \dot{U} \end{Bmatrix} = \{0\} \tag{2}$$

Received Jan. 21, 1995; revision received Aug. 18, 1995; accepted for publication Nov. 14, 1995.

*Research Assistant, Department of Aerospace Engineering, 373-1, Kusong-Dong, Yusong-Gu.

†Associate Professor, Department of Aerospace Engineering, 373-1, Kusong-Dong, Yusong-Gu. Member AIAA.